metals

Article

Removal of Iron, Zinc, and Copper Impurities from Sodium Aluminate After the Bayer Process

Vladimir Damjanović [1], Srećko Stopić [2,*], Duško Kostić [2,3], Mitar Perušić [3], Radislav Filipović [1,3], Aleksandar Mitrašinović [4] and Dragana Kostić [3]

[1] Alumina Ltd., Karakaj 105e, 75400 Zvornik, Republic of Srpska, Bosnia and Herzegovina; vladimir.damjanovic@birac.ba (V.D.); radislav.filipovic@birac.ba (R.F.)
[2] IME Process Metallurgy and Metal Recycling, RWTH Aachen University, 52056 Aachen, Germany; dusko.kostic@tfzv.ues.rs.ba
[3] Faculty of Technology Zvornik, University of East Sarajevo, 75400 Zvornik, Republic of Srpska, Bosnia and Herzegovina; mitar.perusic@tfzv.ues.rs.ba (M.P.); dkostic585@gmail.com (D.K.)
[4] Institute of Technical Sciences of the Serbian Academy of Sciences and Arts, 11000 Belgrade, Serbia
* Correspondence: sstopic@ime-aachen.de

Abstract: This study investigates the influence of specific surface area (SSA) and aluminum hydroxide particle size on sodium aluminate's purification efficiency in the Bayer process. This research examines how variations in SSA affect the adsorption and incorporation of contaminants such as Cu, Fe, and Zn, as well as the optimal balance between effective purification and excessive Al_2O_3 loss. Different SSA values and purification durations are analyzed to optimize the purification process and determine conditions that maximize impurity removal while maintaining system stability. Additionally, solid residue characterization using X-ray diffraction (XRD), scanning electron microscopy (SEM), and energy-dispersive spectroscopy (EDS) provides insights into impurity incorporation mechanisms, including isomorphic replacement, surface adsorption, and co-crystallization. This study highlights key process parameters that influence impurity behavior and crystallization dynamics, offering valuable guidance for refining industrial purification strategies and improving aluminum hydroxide quality.

Keywords: impurities; removal; precipitation; iron; zinc; copper

Academic Editor: Petros E. Tsakiridis

Received: 1 May 2025
Revised: 9 June 2025
Accepted: 11 June 2025
Published: 17 June 2025

Citation: Damjanović, V.; Stopić, S.; Kostić, D.; Perušić, M.; Filipović, R.; Mitrašinović, A.; Kostić, D. Removal of Iron, Zinc, and Copper Impurities from Sodium Aluminate After the Bayer Process. *Metals* **2025**, *15*, 669. https://doi.org/10.3390/met15060669

1. Introduction

The Bayer process is the most commonly used for alumina production, although there are plants operating alternative processes depending on available raw materials (the combined Bayer–sinter process and the Nepheline-based process) [1–3]. Due to different constituents of the raw material, primarily bauxite, the ore needs to be treated to produce alumina of the requested quality (Al_2O_3). This is achieved by blending and grounding it to ensure consistent infeed, which is followed by digestion in autoclaves at high pressures and temperatures, along with caustic soda (NaOH). These conditions are chosen based on the type of aluminum minerals present in the bauxite [4]. The aluminum minerals are selectively dissolved to form an equilibrium, with the conditions driving the reaction from left to right to obtain sodium aluminate ($NaAl(OH)_4$), as represented in the following adapted equations: Equation (1) for gibbsite and Equation (2) for boehmite and diaspore. This stage is called leaching [5].

$$Al(OH)_3 + Na^+ + OH^- \rightleftarrows Al(OH)_4^- + Na^+ \quad (1)$$

$$AlO(OH) + Na^+ + OH^- + H_2O \rightleftarrows Al(OH)_4^- + Na^+ \quad (2)$$

After leaching in the Bayer process stream, the resulting process solution is filtered to remove insoluble residues. These include all other minerals (iron, titanium, silica, and calcium) that are present in bauxite and representing waste called red mud or bauxite residue [6]. The solution is then cooled in crystallizers in the presence of seed crystals of fine $Al(OH)_3$ to precipitate and extract aluminum hydroxide from the sodium aluminate solution. After the precipitation, the mother liquor, rich in sodium hydroxide, is used again in the leaching process. The produced aluminum hydroxide can be heated to around 1000 °C in the calcination process to remove water and produce anhydrous aluminum oxide (alumina), as shown in Equation (3) [7,8]:

$$Al(OH)_3 \rightarrow Al_2O_3 + H_2O \quad (3)$$

The Bayer process for alumina production relies on the stability of aluminate solutions, which is influenced by several key parameters, including concentration, caustic ratio (caustic ratio is the ratio of total sodium oxide (Na_2O) to alumina (Al_2O_3) in the Bayer process), liquor temperature, and the presence of impurities. Industrial aluminate solutions inevitably contain impurities that can affect both their stability and the quality of the final alumina product. However, the precise impact of these impurities remains insufficiently understood. This paper focuses on investigating the process for the removal of these impurities and exploring the mechanisms under which certain impurities could be removed from the liquor [9,10].

Impurities in aluminate solutions can be classified as organic or inorganic. Organic impurities primarily include oxalates, acetates, and bitumen, while inorganic impurities consist of dissolved elements such as Fe^{2+}, Zn^{2+}, Cu^{2+}, Ca^{2+}, Na^+, and $(SiO_3)^{2-}$ [11]. During bauxite leaching at elevated temperatures and pressures, aluminum dissolves into the solution along with certain impurities, which then become part of the aluminate solution. Compared to bauxite processing, in the case of synthetic solutions, which are produced by dissolving the aluminum hydroxide in caustic soda, some impurities originate from dissolved aluminum hydroxide, and this could influence hydroxide precipitation in the next phase. Silica dissolves in the form of sodium silicate (Na_2SiO_3) when exposed to NaOH [12]. Iron, present in bauxite as goethite and hematite, has a very low dissolution rate during leaching, and it can primarily be found as ferrate ions ($Fe(OH)_4^-$) or colloidal particles in aluminate solutions [13]. Zinc, due to its instability in alkaline environments, is usually present in the form of zincate (ZnO_2^{2-} or $Zn(OH)_4^{2-}$), although colloidal zinc may also be formed, making separation by filtration challenging [14,15]. In the Bayer process, copper is present in sodium aluminate solutions as a result of bauxite leaching, where copper-bearing minerals like chalcopyrite dissolve under alkaline conditions. In the highly caustic environment, copper exists primarily in the form of cuprate complexes such as $Cu(OH)_4^{2-}$ or CuO_2^{2-}, and it may also form colloidal particles. These copper species can influence the precipitation of aluminum hydroxide, potentially affecting the purity and properties of the final alumina product [16–19]. In the Bayer process, organic impurities such as sodium oxalate and acetate can accumulate in the aluminate solution, adversely affecting the precipitation of aluminum hydroxide. To address this, researchers have explored the use of alkaline-earth metal carboaluminates, specifically magnesium and calcium hydrocarboaluminates, as effective sorbents for removing these organic contaminants. These compounds exhibit high selectivity towards organic substances, facilitating their removal from the solution and thereby enhancing the purity of the resulting alumina product [20].

Potassium impurities in sodium aluminate solutions can lead to the formation of undesirable compounds during the crystallization process. A single-step crystallization method has

been developed to effectively remove potassium by promoting its incorporation into specific crystalline phases that can be separated from the solution. This approach not only reduces the potassium content but also improves the overall quality of the alumina produced [21].

An experimental study on the purification of aluminate solutions was conducted at Alumina Ltd., demonstrating the successful removal of iron, zinc, and copper from Bayer liquor with over 90% efficiency. The purified solution remained economically viable for further processing, allowing for the production of various types of aluminum trihydrate. The results indicated that increasing the contact time between the liquor and seed crystals enhances the removal of these impurities. However, higher temperatures reduce impurity removal efficiency due to increased solubility and a lower precipitation rate. Optimal impurity removal was achieved at 40 °C [22].

A filtration process using a granular $Fe_2O_3^-$-based substance (40–100 wt.% Fe_2O_3) was effective in removing copper and zinc species from the solution. For improved zinc removal, the Fe_2O_3 particles were coated with a metal sulfide, preferably zinc sulfide (ZnS). In aluminum production, impurity limits are critical, with a maximum allowable zinc content of 0.03 wt.% in certain alloys. To maintain aluminum oxide purity, CuO and ZnO concentrations should be below 0.015 wt.% and 0.023 wt.%, respectively. Reducing impurities such as zinc in Bayer liquor helps obtain alumina with fewer incorporated contaminants in its crystalline structure [23].

Milovanovic et al. [13] studied Bayer liquor purification through crystallization at 52 °C for 24 h, using aluminum hydroxide seed with specific structural properties. The resulting aluminum hydroxide was calcined at 950 °C for 2 h (heating rate: 5 °C/min). The obtained alumina (Alumina I) was compared with alumina produced without Bayer liquor purification (Alumina II) from Alumina Ltd. Zinc concentration in the Bayer liquor was reduced from 0.0494 g/L to 0.0057 g/L after purification. Correspondingly, ZnO content in alumina decreased from 0.026 wt.% (Alumina II) to 0.016 wt.% (Alumina I), highlighting the effectiveness of impurity removal [24].

In our previous work, we developed a three-stage purification strategy to achieve high-purity aluminum hydroxide by systematically removing silica, calcium, iron, zinc, and copper impurities from sodium aluminate solutions and finally removing sodium from the precipitated product. The first stage involved the addition of lime, which effectively reduced silica and calcium to acceptable levels under optimized conditions. In the second stage, specially produced aluminum hydroxide seed crystals facilitated the removal of iron, zinc, and copper, with lower temperatures proving more effective for impurity reduction. Finally, hydrothermal washing was performed to eliminate residual sodium oxide, which is occluded in precipitated alumina trihydrate, where increased time, temperature, and hydrate concentration improved purification efficiency [25].

The novelty of this paper lies in its continuation of our previous research on the purification of sodium aluminate solutions, with a specific focus on the effect of seed crystal particle size and specific surface area on the removal of zinc, copper, and iron impurities. While our prior work demonstrated the effectiveness of seed crystals for impurity removal, this study provides a deeper investigation into how variations in particle size and surface area influence the efficiency of process of purification. By systematically analyzing these parameters, we aim to optimize the purification process, enhancing impurity removal while maintaining process efficiency and cost-effectiveness. This research offers new insights into improving alumina purity and refining industrial Bayer process operations.

2. Materials and Methods

2.1. Materials

Non-metallurgical hydrate obtained at the factory Alumina d.o.o., Zvornik, Republic of Srpska, Bosnia and Herzegovina, was used as raw material to obtain synthetic sodium aluminate solution. For the preparation of seed crystals, we used dried and ground material from the production plant of Alumina Ltd., which is milled on different levels in the mills with beads to reach different micronized levels and specific surface areas shown in Figure 1.

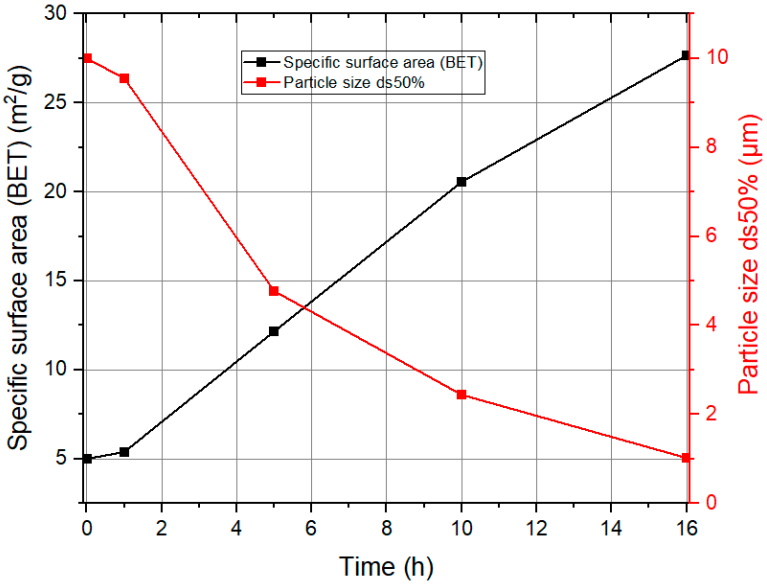

Figure 1. Particle size and specific surface area of ground aluminum hydroxide in correlation with milling time.

Figure 1 illustrates the relationship between grinding time, particle size, and specific surface area of milled (ground) aluminum hydroxide. As grinding time increases, particle size decreases due to the mechanical breakdown of larger particles, leading to finer material. Simultaneously, the specific surface area increases with smaller particles, providing higher total surface area for interaction.

2.2. Methods

The chemical composition of the sample was analyzed using X-ray fluorescence (XRF) spectroscopy on a Shimadzu 8000 device (Shimadzu, Kyoto, Japan). Bulk analysis, with a focus on detecting impurities, was carried out via Atomic Absorption Spectroscopy (AAS) or Inductively Coupled Plasma (ICP) methods. All samples were analyzed under the following conditions: beam voltage of 10 kV, X-ray energy range from 0 to 10 keV, a beam frequency of 20,000 pulses per second, and an acquisition time of 300 s. Composition identification was done using the DIFFRAC.SUITE EVA FT software, Version 4.2.

Scanning electron microscope (SEM) analysis was conducted on a JSM 7000F by JEOL (manufactured in 2006, JEOL Ltd., Tokyo, Japan), and energy-dispersive X-ray (EDX) analysis was performed using an Octane Plus-A detector by Ametek-EDAX (manufactured in 2015, AMETEK Inc., Berwyn, PA, USA) with Genesis V 6.53 software. The results revealed an irregular structure in the solid residue.

X-ray Diffraction (XRD) analysis of the solid residue from the first purification phase was carried out using a Bruker D8 Advance equipped with a LynxEye detector (Bruker AXS, Karlsruhe, Germany). X-ray powder diffraction patterns were recorded using a Bruker AXS D4 Endeavor diffractometer in Bragg–Brentano geometry (Bruker AXS, Karlsruhe,

Germany), fitted with a copper tube and a primary nickel filter, providing Cu Kα1,2 radiation (λ = 1.54187 Å).

2.3. Procedure

To achieve the highest quality aluminum hydroxide, it is essential to purify the aluminate solution by removing the various impurities it contains. The amount of organic and inorganic impurities dissolved in sodium aluminate in the Bayer process depends on several factors, including temperature, bauxite type and composition, pressure, and other operational parameters. These factors determine the extent of impurity dissolution in the sodium aluminate solution. In Table 1, the design of the experiments is shown.

Table 1. Design of the experiments.

Experiment No.	Seed Crystal Particle Size (μm)	SSA of Seed Crystal (m^2/g)	Time (min)
1	9.55	5.3897	30
2	9.55	5.3897	60
3	9.55	5.3897	90
4	9.55	5.3897	120
5	4.77	12.1691	30
6	4.77	12.1691	60
7	4.77	12.1691	90
8	4.77	12.1691	120
9	2.44	20.5632	30
10	2.44	20.5632	60
11	2.44	20.5632	90
12	2.44	20.5632	120
13	1.02	27.6645	30
14	1.02	27.6645	60
15	1.02	27.6645	90
16	1.02	27.6645	120

Through empirical research, it was determined that 200 g of solid NaOH per liter of demineralized water is required to dissolve 260 g of non-metallurgical hydrate. This results in an aluminate solution with concentrations of 174 g/L of Al_2O_3 and 155 g/L of Na_2O, which was then subjected to purification.

The purification process for removing these impurities was conducted as outlined in Figure 2.

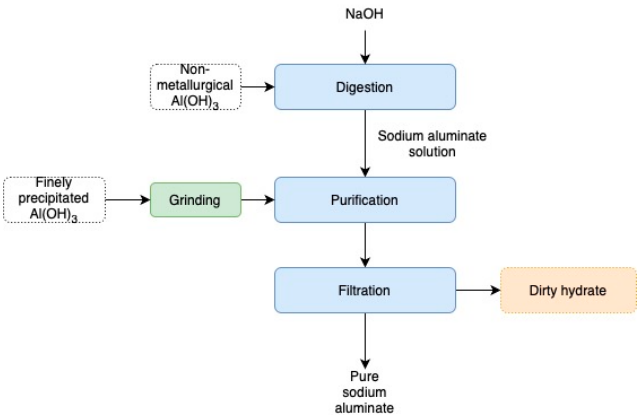

Figure 2. Block scheme of the purification process.

The figure illustrates the overall process for purifying aluminum hydroxide, which will be presented in this paper. It begins with non-metallurgical aluminum hydroxide, which is digested with sodium hydroxide (NaOH) to produce a sodium aluminate solution. This solution, which contains various impurities, requires purification to achieve the desired quality of aluminum hydroxide.

The first step in the purification process involves grinding finely precipitated hydrate with varying grinding times and particle sizes, as outlined in the materials section of the paper. These different particle sizes (specific surface area) are crucial as they affect the purification process. The ground hydrates are then mixed with the sodium aluminate solution, and the effect of different particle sizes, or specific surface areas, on the purification efficiency over time is investigated.

Following the mixing and reaction, the next stage is filtration. The filtration process separates the solid phase, which contains the impurities and the ground hydrates, from the liquid phase (purified sodium aluminate solution).

Preparation of Tablets

This method involves immersing the sample in epoxy resin, and then the samples are polished with water-sanding abrasive paper to cut the agglomerated and layered particles. A small amount of powder was placed in molds measuring 4 × 4 cm, and then the sample was immersed in epoxy resin and left for 12 h to harden. After the sample hardened, it was removed from the mold and polished. The sample thus prepared was then reanalyzed on a scanning electron microscope, where EDS point analysis was also performed, to determine the composition. Polishing of the samples was done with water-sanding papers of different grain fineness with water. Polishing with sandpapers of different fineness was done in the following order (from coarser to finer granulations): 46 μm > 30 μm > 18 μm > 10 μm > 5 μm. The duration of each operation amounted to 15 min.

3. Results

3.1. Liquid Phase Results

Influence of the Specific Surface Area of Finely Precipitated Hydrate

After completing the experiments, the obtained results were analyzed to evaluate the influence of the specific surface area of finely precipitated hydrate on the purification process.

In Figure 3a, the concentrations of Cu and Fe show a sharp decline within the first 30 min of purification, indicating an efficient removal process even with the smallest specific surface area of 5.3897 m^2/g. This suggests that the purification method effectively adsorbs and eliminates these impurities at an early stage. In contrast, Zn concentration decreases at a much slower rate, implying that its removal is less efficient compared to Cu and Fe see Table A1.

Figure 3b shows that sodium hydroxide concentration (Na_2O content) remains stable throughout the purification process, indicating that it does not participate in the crystallization or adsorption reactions. However, the alumina concentration (Al_2O_3 content) gradually decreases over time due to the crystallization process. This occurs because the added aluminum hydroxide, which acts as a seed crystal, promotes further crystallization, and it also acts as an adsorbent for impurity adsorption. As a result, the caustic modulus, which represents the molar ratio of Na_2O to Al_2O_3, increases gradually over time. However, this increase is not significant, suggesting that under these process conditions (concentration of reactants and seed crystals), the kinetics of the crystallization process is not so fast and does not cause major structural transformations in the system.

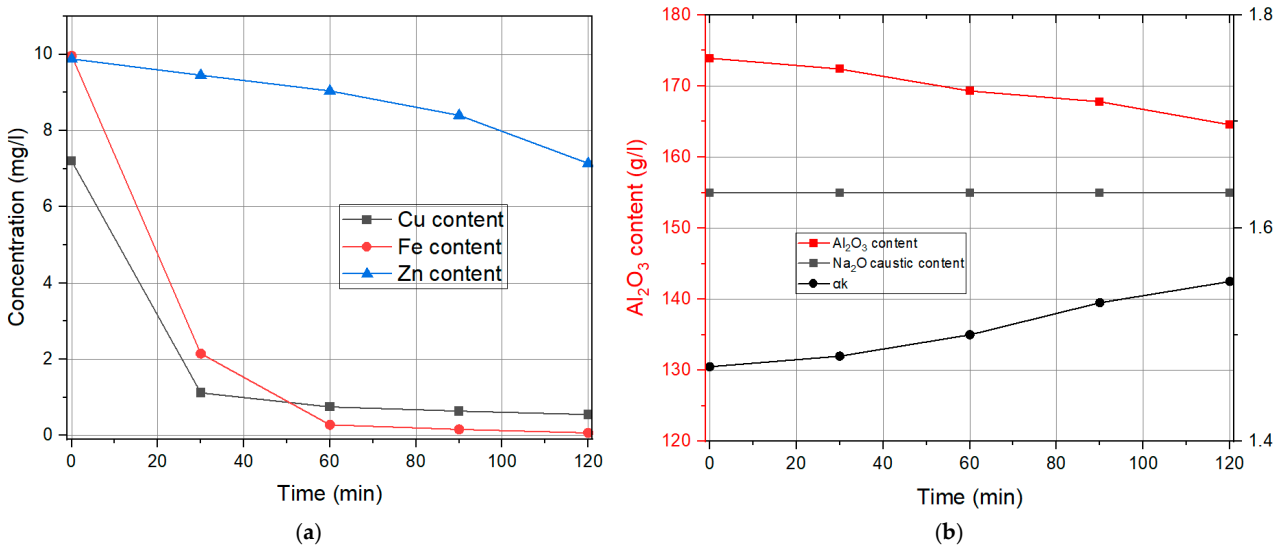

Figure 3. (**a**) Variation in Cu, Fe, and Zn concentration over purification time. (**b**) Changes in caustic modulus during purification for SSA of seed crystals of 5.3897 m^2/g.

In Figure 4a, the concentrations of Cu and Fe decrease significantly within the first 30 min, similar to the trend observed at a lower SSA of seed crystals. However, with an increased SSA of seed crystal to the value of 12.1691 m^2/g, the Zn content also decreases more over time, indicating improved adsorption efficiency. The enhanced removal of Zn suggests that a larger surface area provides more active sites for adsorption, leading to better overall impurity reduction (see Table A2).

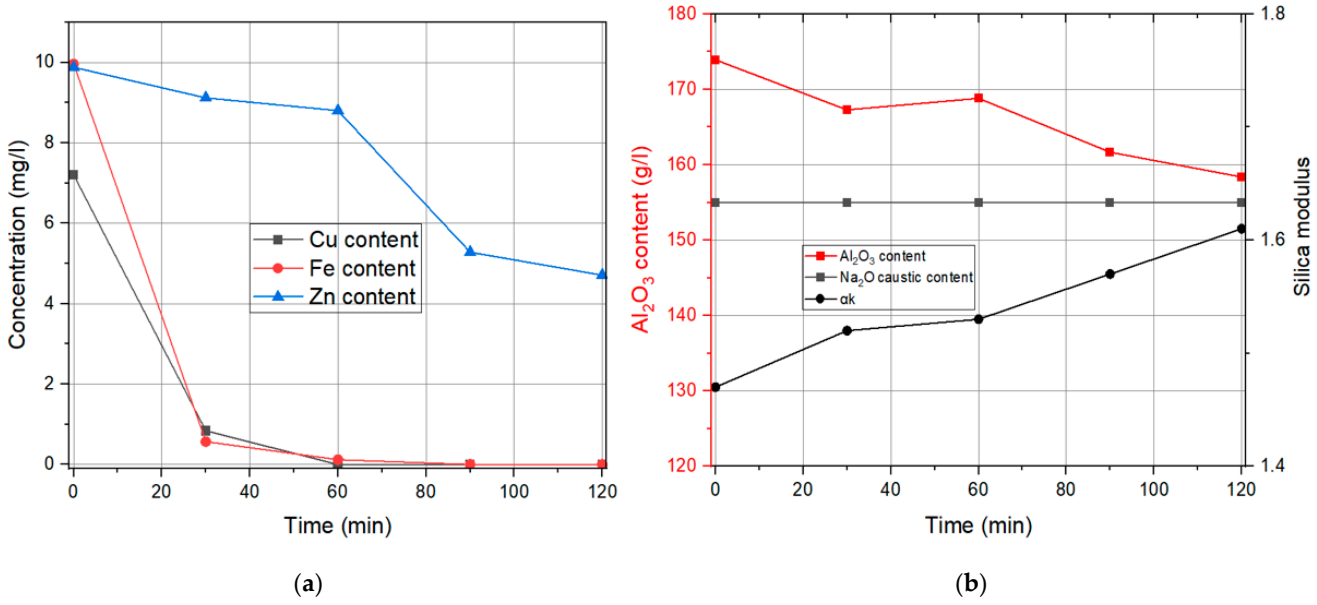

Figure 4. (**a**) Variation in Cu, Fe, and Zn concentration over purification time. (**b**) Changes in caustic modulus during purification for SSA of seed crystals 12.1691 m^2/g.

In Figure 4b, the crystallization process becomes more intensive with the use of seed crystals with higher SSA, leading to a more noticeable decrease in alumina concentration in sodium aluminate liquor (Al_2O_3 content) over time. The ground hydrates, which serve as seed crystals, promote more extensive crystallization, increasing the kinetics of the process. The reason for this lies in the higher activation energy that is introduced in a system with a seed of higher SSA under the same concentration of added seed. With the rise of SSA, the

system experiences stronger crystallization effects, leading to a continuous increase in the caustic modulus over the reaction time.

In Figure 5a, the concentrations of Cu and Fe drop to 0 within the first 30 min, showing an even higher efficiency compared to the use of seed crystals with lower SSA values. The Zn content also shows a significant decline, reaching near-complete removal by the end of the purification process. This improvement highlights the strong influence of SSA on adsorption efficiency, as a larger surface area provides more active sites for impurity removal, allowing for faster and more complete purification (see Table A3).

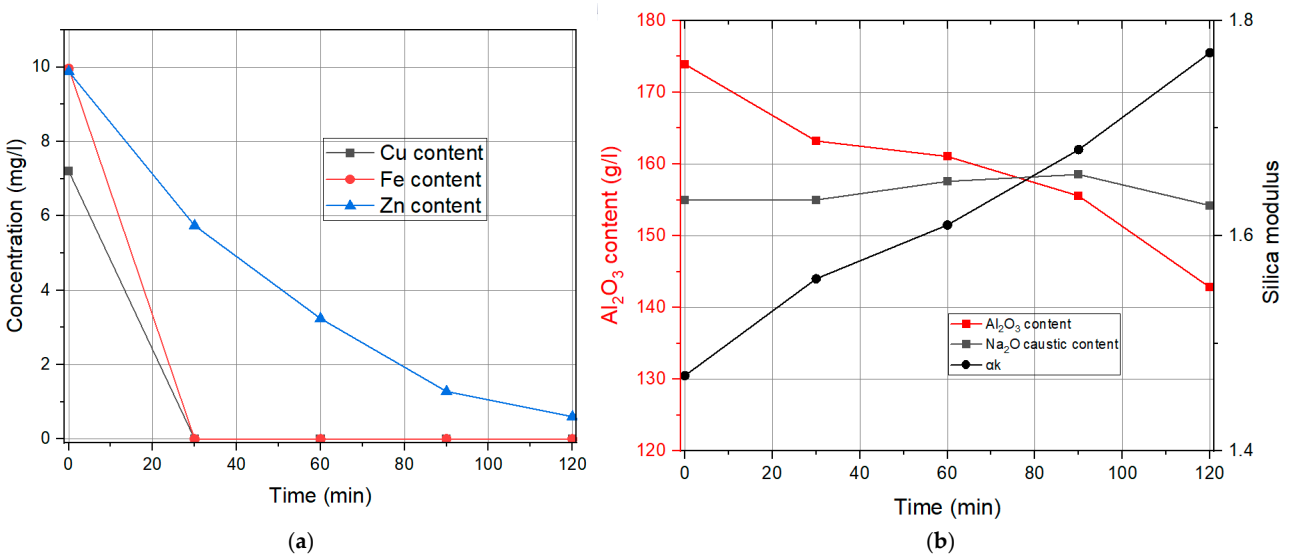

Figure 5. (**a**) Variation in Cu, Fe, and Zn concentration over purification time. (**b**) Changes in caustic modulus during purification for SSA of seed crystals 20.5632 m^2/g.

In Figure 5b, the crystallization process becomes even more intense with the use of seed crystals with a higher SSA of 20.5632 m^2/g. Values of alumina concentration in the liquor (Al_2O_3) show a steeper decline over time, indicating continuous and faster crystallization, showing these seed crystals even more active during the process. Unlike previous cases, the concentration of sodium hydroxide (Na_2O) is no longer constant but begins slight increase slightly after 60 min. Since the concentrations of caustics should be stable, reason for the slight increase is evaporation, since the process is at atmospheric pressure. The caustic modulus experiences a rapid and significant rise, reflecting the faster process of crystallization in the case of seed crystals with higher SSA. The rapid increase in caustic modulus suggests that in the case of the use of higher SSA of seed crystals, the system undergoes substantial structural changes, and with the increase in time, a significant loss of alumina from the liquor is detected.

In Figure 6a, the concentrations of Fe and Cu drop to zero within the first 30 min, confirming the highly efficient removal of these impurities. The Zn content also significantly decreases, reaching zero at 120 min, demonstrating that in the case of seed crystals with SSA of 27.6645 m^2/g, the purification process is 100% for all three elements Table A4.

In Figure 6b, the caustic ratio increases to very high values, indicating an intensified crystallization process. The Al_2O_3 content in the liquor decreases over time, as in the previous cases, reaching a very low level of 133 g/L at 120 min. Such a significant reduction suggests that prolonged purification with seed crystals at high SSA can lead to excessive crystallization, which may lead to high precipitation yield and it could be a big loss if the next steps are planned in further processing. Therefore, optimization of the purification time is crucial. At 90 min, a good balance is achieved, with effective Zn removal and an Al_2O_3 content of 151 g/L, ensuring efficient purification while maintaining a stable process.

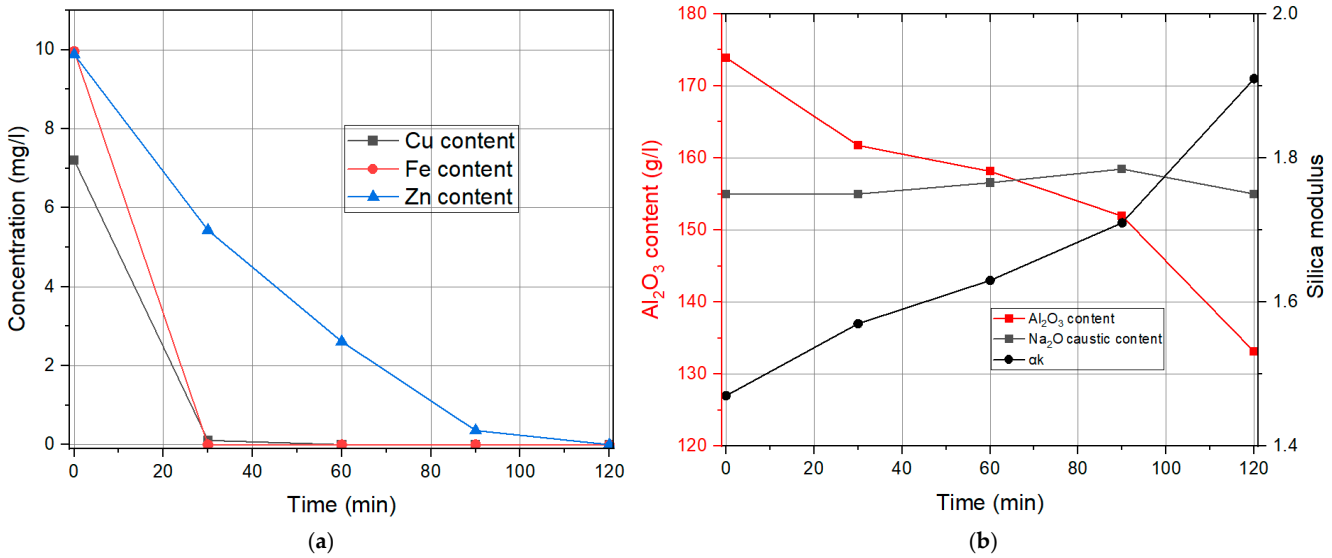

Figure 6. (**a**) Variation in Cu, Fe, and Zn concentration over purification time. (**b**) Changes in caustic modulus during purification for SSA of seed crystals 27.6645 m^2/g.

3.2. Solid Residue Results

The incorporation of zinc into the aluminum hydroxide structure is a crucial aspect of the process that affects the purity of the obtained crystals. During the crystallization of aluminum hydroxide, zinc has the potential to be included in the crystal lattice or to be adsorbed on the surface of the crystal, which depends on the process conditions and the chemical environment. There are several mechanisms that can explain the incorporation of zinc, iron, and other components of the solution. Isomorphic replacement: Zinc ions can replace ions of aluminum in the crystal lattice, which occurs due to the similarity in ion size and chemical characteristics. This type of substitution is more intense when the crystallization conditions are rapid and uncontrolled. Surface adsorption: Zinc can be adsorbed on the surface of formed crystals under certain conditions, especially in cases where the crystal surface is larger than its volume, which is the case with smaller crystals. Co-crystallization: In some cases, zinc can co-crystallize with aluminum hydroxide, forming mixed crystals if the conditions for its crystallization are favorable. Factors such as pH value, zinc concentration in the solution, presence of other ions, and temperature directly affect the degree and manner of incorporation. The control of these parameters is essential to reduce unwanted incorporation, thereby ensuring a higher level of aluminum hydroxide purity. Examining and understanding these processes is crucial for optimizing methods for zinc removal and improving the quality of the final product in industrial applications. Given the various mechanisms of zinc incorporation into the structure of precipitated aluminum hydroxide, we tried to determine whether there is any other mineralogical structure besides the expected gibbsite aluminum trihydrate by X-ray structural analysis. Figure 7 shows the diffractogram of the analyzed sample (5B: 120 min, 50 °C, 5 g/L).

Unfortunately, this instrumental technique did not determine the presence of another mineral structure except for the expected aluminum hydroxide. There are two possible reasons for this. The first is that there was no crystallization of the other mineral structure due to the fact that the concentration of zinc in the solution was very low, just like iron. In addition, the chemical analysis also determined a small concentration of these elements in the precipitated aluminum hydroxide, which could potentially limit the detection by this method. SEM analysis of a sample of the solid residue after zinc removal is given in Figure 8.

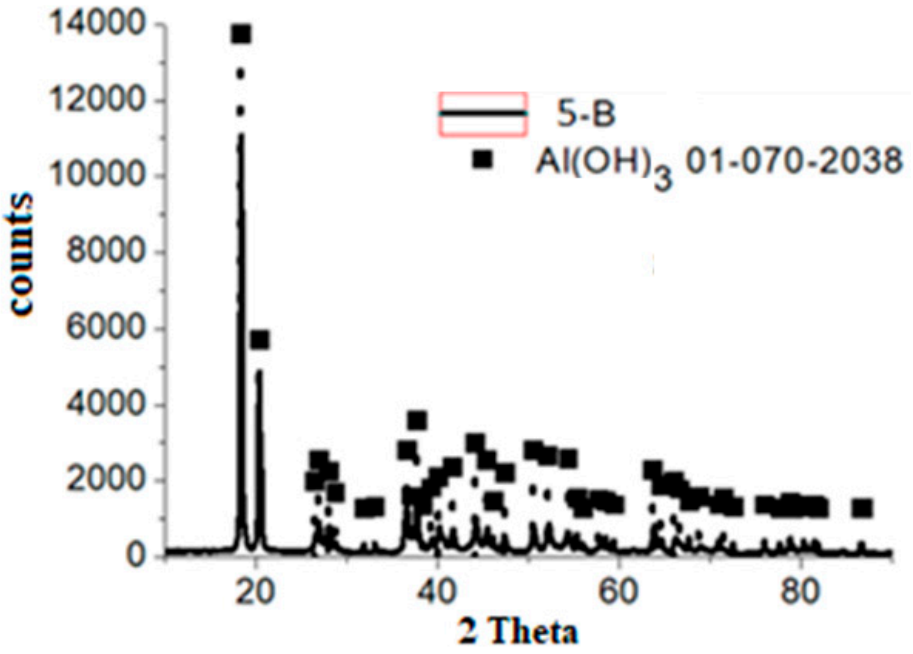

Figure 7. XRD analysis of the sample obtained at 120 min, 50 °C, 5 g/L.

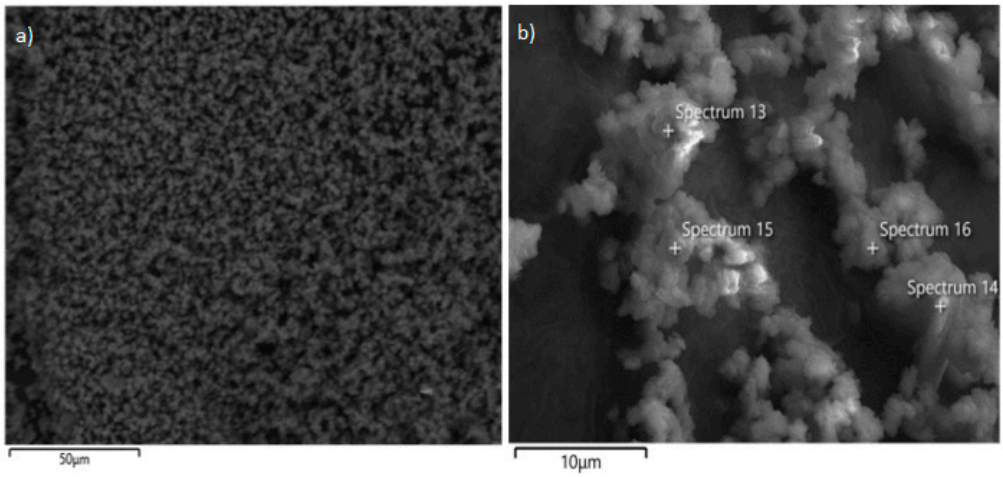

Figure 8. SEM analysis of solid residue from Exp. (120 min, 50 °C, 5 g/L) (**a**) for a 50 µm scale indicator, (**b**) for a 10 µm scale indicator.

In Figure 9, an individual presentation of individual elements through EDS mapping is given.

As can be seen from the results of the EDS mapping analysis, aluminum is the most dominant, which corresponds to the results shown earlier, because aluminum hydroxide is also the expected product of the reaction.

Figure 10 shows the SEM analysis of the solid residue after the process of removing zinc from the solution at a temperature of 50 °C, a time of 120 min, and an amount of added seed crystal of 5 g/L.

The image clearly shows that the obtained particles are agglomerated and irregularly shaped, significantly larger than 1 µm. This is also confirmed by the results of the PSD analysis, where the mean diameter of the size of the obtained particles was detected as 2.96 µm, which is almost six times larger than the mean diameter of the starting particles of 0.47 µm. On that occasion, an EDS point analysis was performed on the given sample, where the chemical content was checked at certain points on the sample. In addition to

aluminum hydroxide from XRD analysis, the presence of sodium was also determined. This was also confirmed by the EDS analysis of the given sample during mapping, which is shown in Figure 11a. It can be seen that the sodium concentration was determined at the level of 0.5%, which approximately corresponds to the results of the chemical analyses previously performed on this sample.

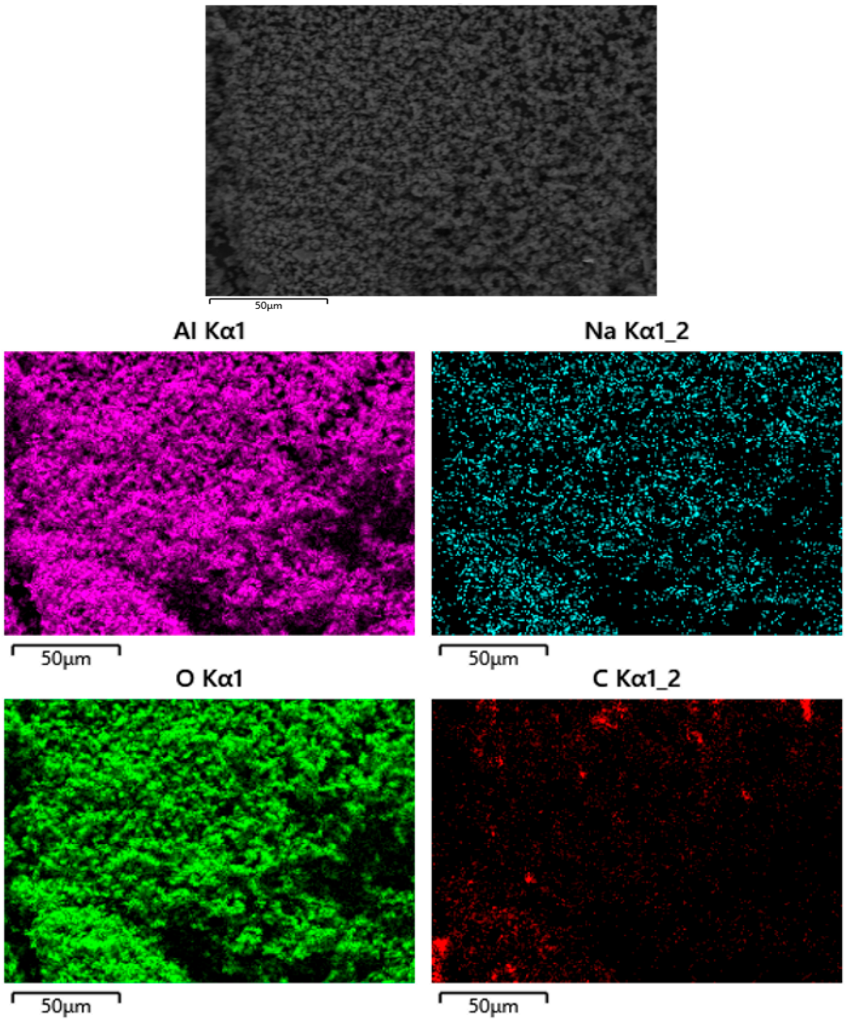

Figure 9. EDS mapping of cations of individual elements in the sample.

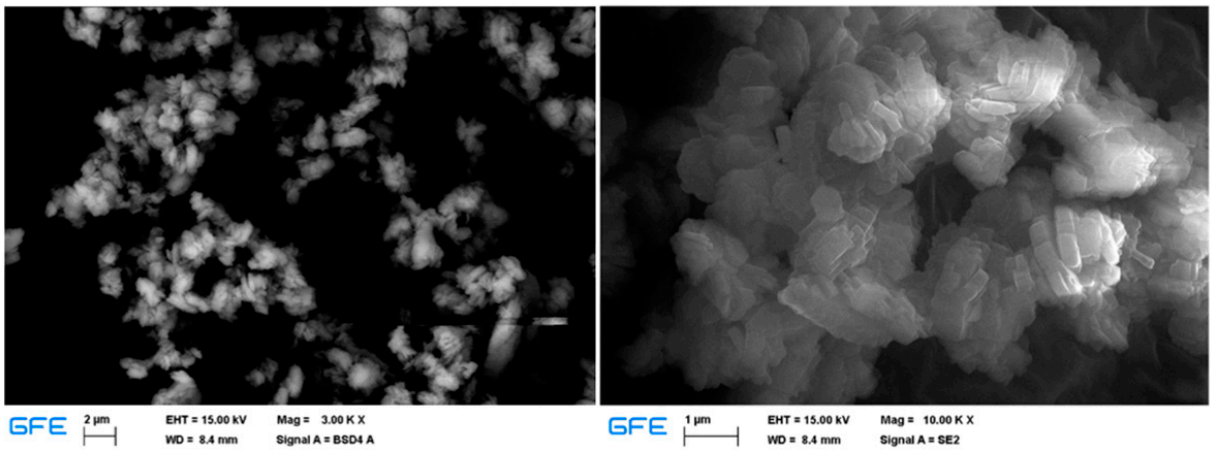

Figure 10. SEM analysis of powders after the second stage of purification, zinc and iron removal at different magnifications (5B: 120 min, 50 °C, 5 g/L).

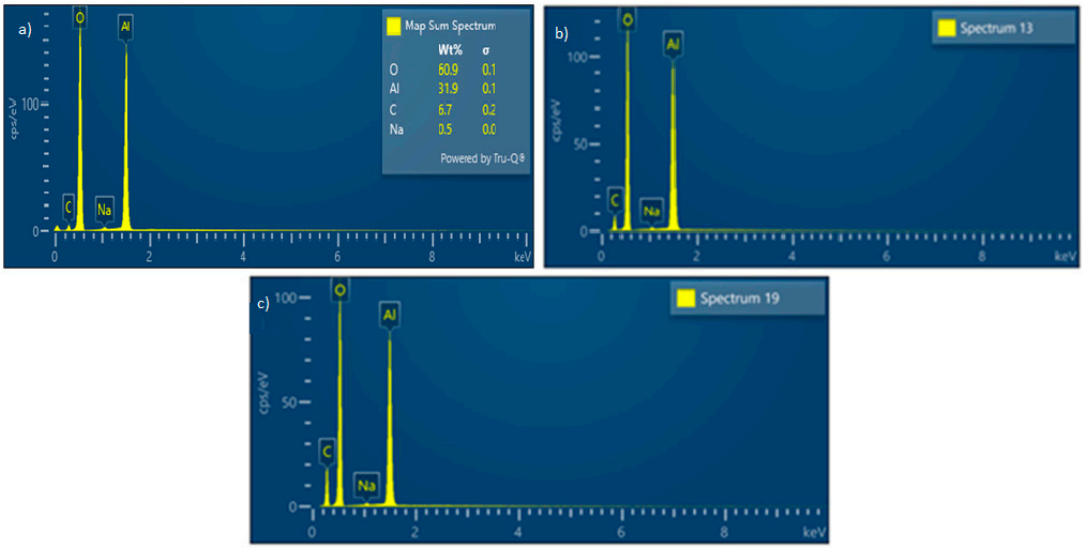

Figure 11. Quantitative EDS analysis of the sample (120 min; 50 °C, 5 g/L) (**a**) from the solid residue during mapping of the scanned part, (**b**) spectrum 13 from Figure 8b, (**c**) spectrum 19.

Based on the results shown in Figures 11, A1 and A2, it can be seen that during the surface EDS point analysis, the main components are aluminum, originating from aluminum hydroxide, and sodium, which was found as it was in concentrations of 0.5%, and probably in a certain amount, it was adsorbed or remained due to insufficient washing of the obtained particles during filtration. Unfortunately, impurities were not detected with this technique because they were obviously not concentrated on the surface of the material but incorporated into the inner layers or between the agglomerated particles. That is why it was necessary to change the method of preparing samples for imaging on the electron microscope.

Figure 12 shows a photograph at a scale indicator of 1, 25, and 50 μm, and the EDS analysis was performed at five points. The results are shown in Figure 13c. In addition to aluminum (Al), iron (Fe), copper (Cu), calcium (Ca), silicon (Si), but also zirconium (Zr) (Figure A5d), which was not detected in previous cases, were detected in these points. Based on these results, it is concluded that the mentioned aluminum-hydroxide trace elements are concentrated in specific places in the sample, which may indicate material heterogeneity or different phases in the sample. The heterogeneity of the composition of the material in the section, as well as the specific places of presence of the mentioned impurities, indicate that these elements are integrated in the structure of aluminum hydroxide.

The results of the EDS analysis, shown in Figure 13a, show that aluminum oxide ($Al(OH)_3$) dominates in all points, which is expected because controlled crystallization of aluminum hydroxide was performed. However, in these points, in addition to aluminum, sodium (Na), zinc (Zn), iron (Fe), sulfur (S), silicon (Si), and chlorine (Cl) were detected in traces. Chlorine appearing in all spectra originates from the epoxy resin and should be ignored. The presence of these elements and the percentage content during the EDS analysis of the polished surface is variable, indicating an inhomogeneous distribution of impurities in the analyzed powders (Figure A3). Figure 13b shows a snapshot with a scale indicator of 50 μm, and the EDS analysis was done at two points, while the third spectrum is the result of mapping one part of the surface. The EDS results are shown in Figures 13b and A4. In this case, in addition to aluminum as the dominant species, a larger amount of calcium (Ca) was detected at one point. At this point (Spectrum 18), as in Figure A4, calcium is the dominant phase, probably in the form of calcite, while aluminum (Al) is in a significantly lower concentration. In addition to these two elements, silicon (Si) and magnesium (Mg) are also present in traces. Interestingly, calcium was not detected during the XRD analysis of the

sample. This was expected because during the chemical analysis, it was found in very low concentrations in the sample, which is beyond the detection range of the mentioned device. On the other hand, dominant aluminum was again detected on Spectrum 19, with traces of silicon and sodium, which further supports the hypothesis of variability and heterogeneity of the material. Mapping of the sample's surface prepared in this way (Spectrum 20) again indicated the heterogeneity of the composition in the analyzed samples. In this case, iron was detected to a greater extent in addition to aluminum as the dominant element. Besides iron, copper (Cu), barium (Ba), antimony (Sb), zinc (Zn), and calcium (Ca) were also detected.

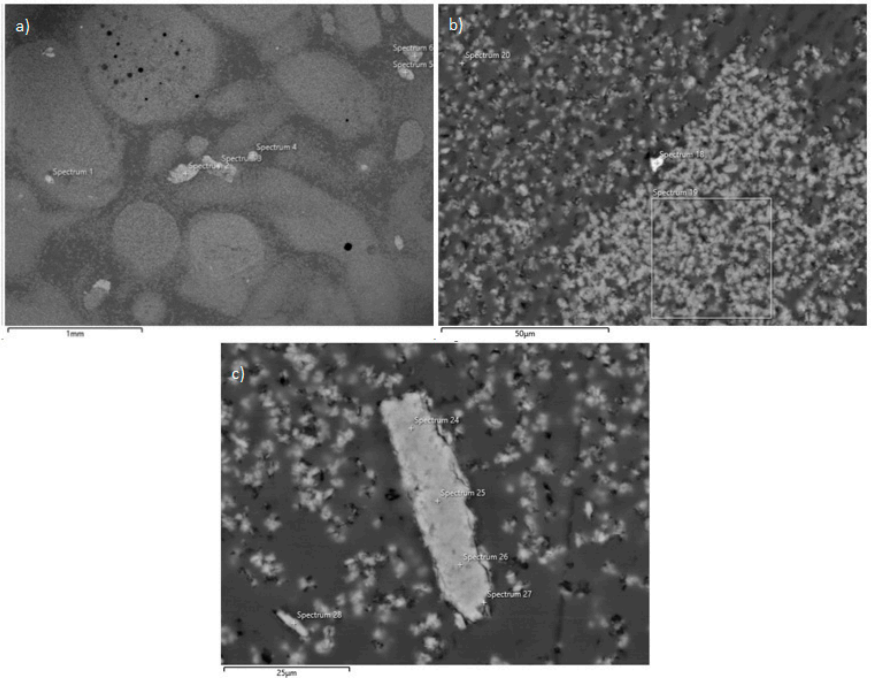

Figure 12. SEM image of polished samples immersed in epoxy resins during EDS analysis for 30 min, 50 °C, 5 g/L (**a**) for a 1 mm scale indicator, (**b**) for a 50 µm scale indicator, (**c**) for a 25 µm scale indicator.

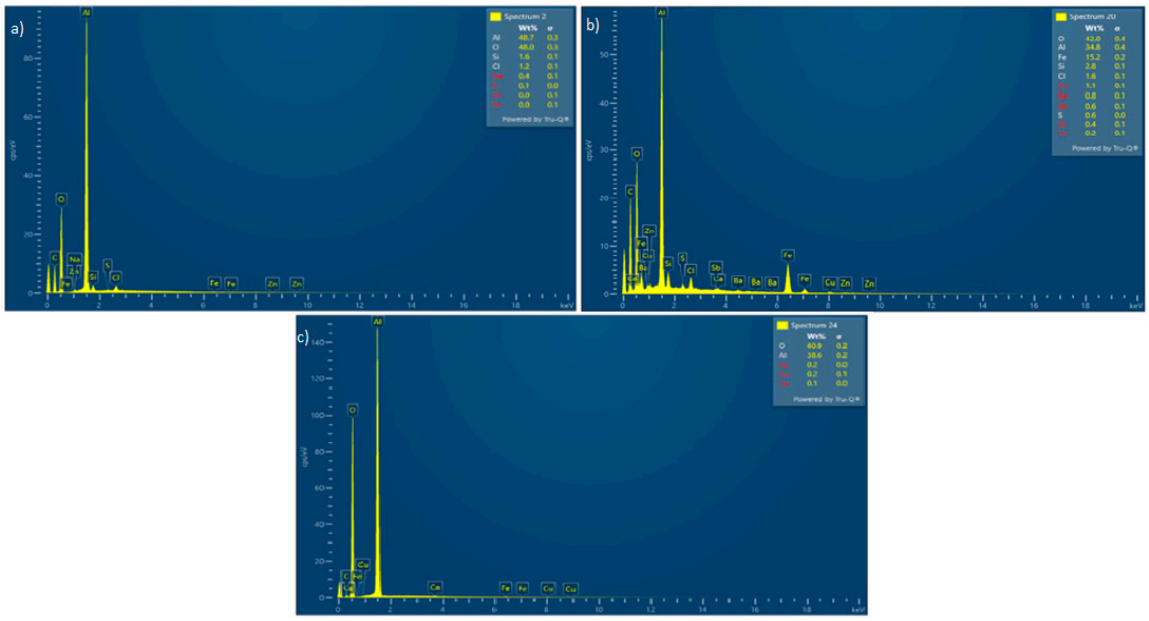

Figure 13. EDS analysis of the sample (30 min, 50 °C, 5 g/L) (**a**) spectrum 2 from Figure 12a, (**b**) spectrum 20 from Figure 12b, (**c**) spectrum 24 from Figure 12c. In the cross-section shown in Figure 13a, analysis was performed with a scale indicator of 1 mm.

4. Conclusions

The results demonstrate that the specific surface area (SSA) of finely precipitated hydrates plays a crucial role in the efficiency of the purification process. As SSA increases, the removal of Cu, Fe, and Zn improves significantly, with Cu and Fe being eliminated within the first 30 min at higher SSA values, while Zn shows a more gradual decline. The enhanced impurity removal is attributed to the increased number of active adsorption sites available at larger SSA, which facilitates more effective interaction with contaminants.

Additionally, the crystallization process intensifies with increasing SSA, leading to a continuous decline in Al_2O_3 content over time. While higher SSA promotes more extensive crystallization and enhances impurity removal, excessive crystallization at prolonged purification times results in a significant loss of Al_2O_3. This is evident at the highest SSA of 27.6645 m^2/g, where the Al_2O_3 content drops to a critical level of 133 g/L after 120 min, indicating potential negative effects on system stability.

Optimization of purification time is essential to balance impurity removal and maintain stable Al_2O_3 content. The results suggest that a purification duration of approximately 90 min is optimal, ensuring efficient Zn removal while maintaining Al_2O_3 at an acceptable level of 151 g/L. This study highlights the importance of controlling SSA and purification time to achieve the best purification efficiency while preventing excessive crystallization losses.

Further analysis of the solid residue offers deeper insights into impurity incorporation mechanisms. The incorporation of Zn into the aluminum hydroxide structure is influenced by process conditions and chemical environment, occurring through isomorphic replacement, surface adsorption, and co-crystallization. Isomorphic replacement, where Zn substitutes for Al in the lattice, is more pronounced under rapid crystallization conditions. Surface adsorption is particularly evident in smaller crystals with larger surface area-to-volume ratios. Co-crystallization, on the other hand, occurs under favorable precipitation conditions, forming mixed phases with aluminum hydroxide. Factors such as pH, Zn concentration, the presence of competing ions, and temperature play a crucial role in determining the extent and mechanism of incorporation.

X-ray diffraction (XRD) analysis of the solid residue confirmed that the primary crystallized phase was aluminum hydroxide, without evidence of other mineralogical structures. However, scanning electron microscopy (SEM) and energy-dispersive spectroscopy (EDS) analyses provided further details on impurity distribution. SEM images revealed agglomerated and irregularly shaped particles with a significant increase in mean particle size from 0.47 μm to 2.96 μm after purification. EDS mapping confirmed the presence of Al as the dominant element, alongside minor amounts of Na, Zn, Fe, S, Si, and Cl. The presence of Na at 0.5% concentration suggests partial adsorption or insufficient washing of particles during filtration.

More detailed EDS point analysis of polished cross-sections further confirmed the heterogeneity of impurity distribution. While $Al(OH)_3$ remained the dominant phase, elements such as Fe, Cu, Ca, Ba, Sb, and Zr were detected in localized regions, suggesting that these impurities are not evenly distributed but rather integrated into specific sites within the aluminum hydroxide structure. Notably, Ca, which was not detected in XRD analysis, was identified in trace amounts in EDS, likely due to its low concentration being below XRD detection limits. The presence of Zn, Fe, and Cu in isolated regions reinforces the hypothesis that impurities are incorporated within the structure rather than forming separate phases. Overall, this study highlights the importance of optimizing SSA and purification duration to maximize impurity removal while preventing excessive crystallization losses.

Author Contributions: Conceptualization, V.D. and D.K. (Duško Kostić); methodology, R.F.; software, A.M. and D.K. (Dragana Kostić); validation, R.F., D.K. (Duško Kostić) and D.K. (Dragana Kostić); formal analysis, V.D., A.M. and D.K. (Dragana Kostić); investigation, R.F., S.S., M.P. and D.K. (Duško Kostić); resources, V.D., S.S. and R.F.; data curation, A.M., V.D. and S.S.; writing—original draft preparation, D.K. (Duško Kostić) and D.K. (Dragana Kostić); writing—review and editing, V.D., M.P., S.S. and A.M.; visualization, D.K. (Duško Kostić), A.M.; supervision, S.S., R.F. and M.P.; project administration, D.K. (Dragana Kostić), S.S. and A.M.; funding acquisition, R.F. and M.P. All authors have read and agreed to the published version of the manuscript.

Funding: This research received no external funding.

Data Availability Statement: The original contributions presented in this study are included in the article. Further inquiries can be directed to the corresponding author.

Conflicts of Interest: Authors Vladimir Damjanović and Radislav Filipović were employed by Alumina Ltd. The remaining authors declare that the research was conducted in the absence of any commercial or financial relationships that could be construed as a potential conflict of interest.

Appendix A

Table A1. Variation in Cu, Fe, and Zn concentration, caustic modulus, and Al_2O_3, Na_2O_c (Caustic) content with purification time for SSA of seed crystals of 5.3897 m^2/g.

Time	Cu Content	Fe Content	Zn Content	Na_2O_c	Al_2O_3	αk
min	mg/L	mg/L	mg/L	g/L	g/L	/
0	7.2	9.96	9.88	155	173.91	1.47
30	1.12	2.15	9.45	155	172.38	1.48
60	0.75	0.28	9.04	155	169.3	1.5
90	0.64	0.16	8.4	156.55	167.79	1.53
120	0.55	0.07	7.14	155	164.54	1.55

Table A2. Variation in Cu, Fe, and Zn concentration, caustic modulus, and Al_2O_3, Na_2O_c content with purification time for SSA of seed crystals of 12.1691 m^2/g.

Time	Cu Content	Fe Content	Zn Content	Na_2O_c	Al_2O_3	αk
min	mg/L	mg/L	mg/L	g/L	g/L	/
0	7.2	9.96	9.88	155	173.91	1.47
30	0.84	0.57	9.12	155	167.28	1.52
60	0	0.12	8.8	157.32	168.81	1.53
90	0	0	5.28	155	161.67	1.57
120	0	0	4.71	155	158.37	1.61

Table A3. Variation in Cu, Fe, and Zn concentration, caustic modulus, and Al_2O_3, Na_2O_c content with purification time for SSA of seed crystals of 20.5632 m^2/g.

Time	Cu Content	Fe Content	Zn Content	Na_2O_c	Al_2O_3	αk
min	mg/L	mg/L	mg/L	g/L	g/L	/
0	7.2	9.96	9.88	155	173.91	1.47
30	0	0	5.74	155	163.2	1.56
60	0	0	3.24	157.58	161.05	1.61
90	0	0	1.28	158.54	155.55	1.68
120	0	0	0.6	154.22	142.8	1.77

Table A4. Variation in Cu, Fe, and Zn concentration, caustic modulus, and Al_2O_3, Na_2O_c content with purification time for SSA of seed crystals of 27.6645 m^2/g.

Time	Cu Content	Fe Content	Zn Content	Na_2O_c	Al_2O_3	αk
min	mg/L	mg/L	mg/L	g/L	g/L	/
0	7.2	9.96	9.88	155	173.91	1.47
30	0.11	0	5.43	155	161.73	1.57
60	0	0	2.61	156.55	158.13	1.63
90	0	0	0.36	158.45	151.92	1.71
120	0	0	0	155	133.11	1.91

Appendix B

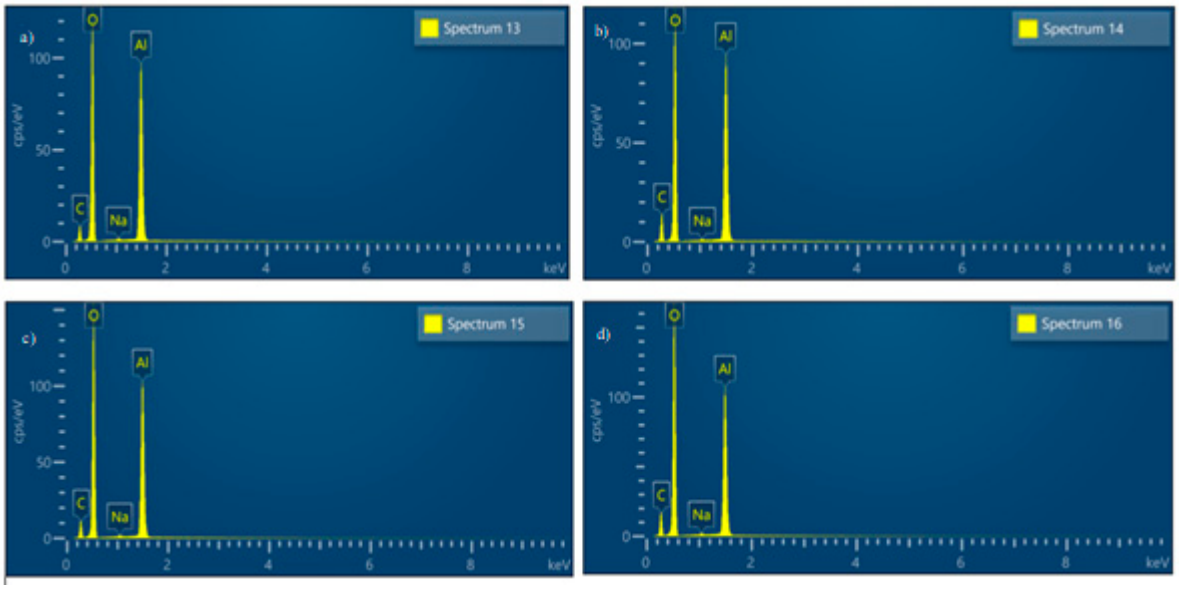

Figure A1. Quantitative EDS analysis of the sample (120 min, 50 °C, 5 g/L) (**a**) spectrum 13, (**b**) spectrum 14, (**c**) spectrum 15 and (**d**) spectrum 16.

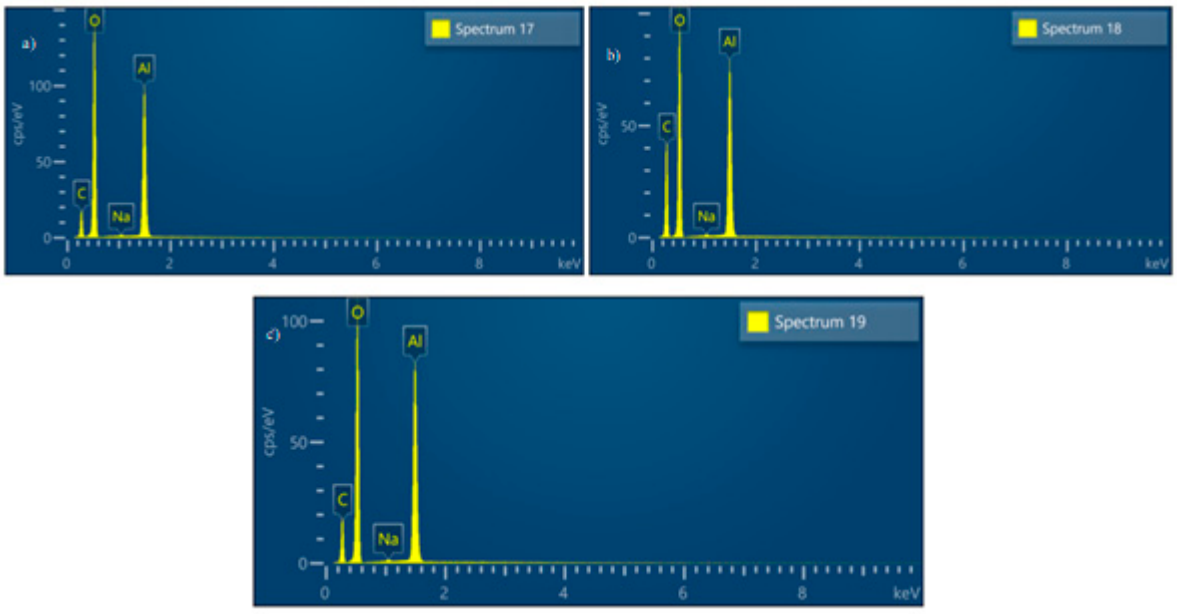

Figure A2. Quantitative EDS analysis of the sample (120 min, 50 °C, 5 g/L) (**a**) spectrum 17, (**b**) spectrum 18, (**c**) spectrum 19.

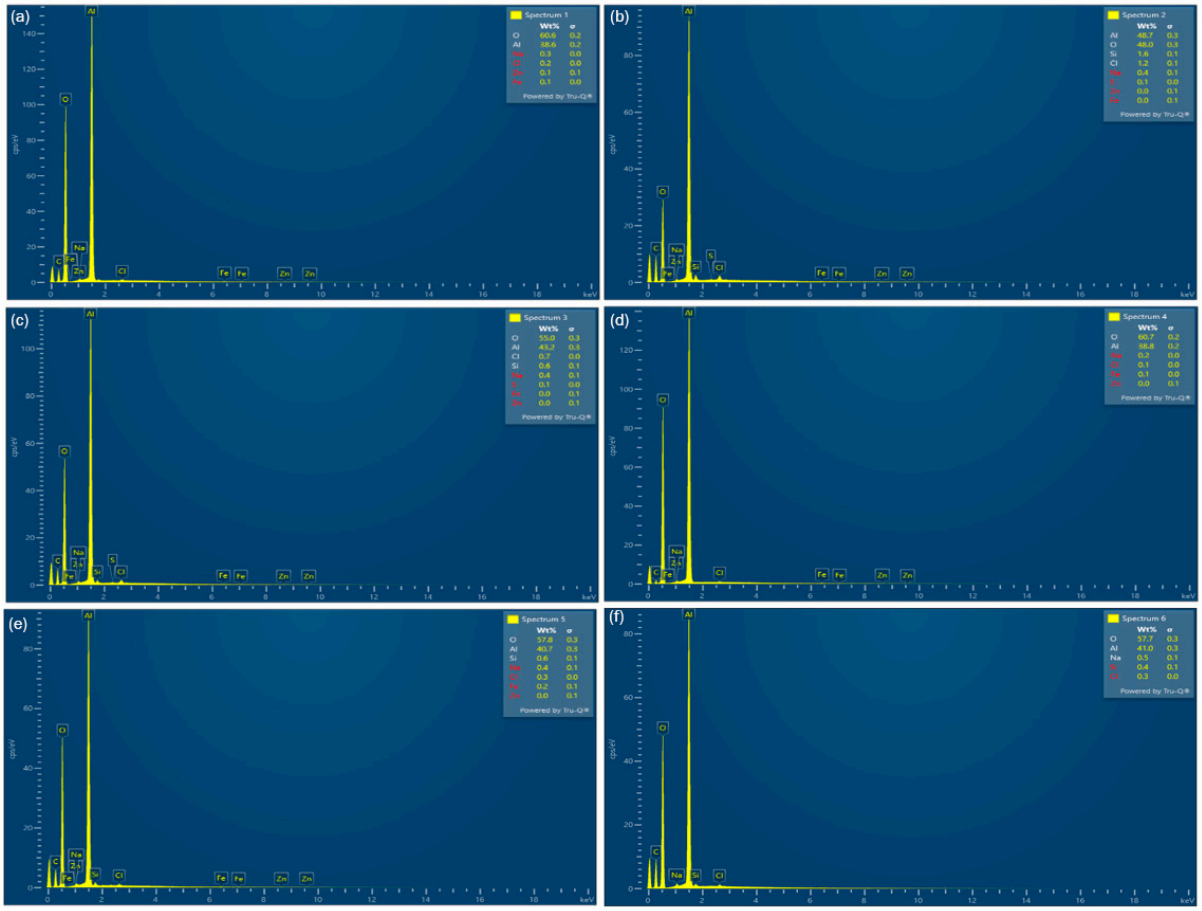

Figure A3. Quantitative EDS of polished samples (30 min; 50 °C, 5 g/L) (**a**) spectrum 1, (**b**) spectrum 2, (**c**) spectrum 3, (**d**) spectrum 4, (**e**) spectrum 5, (**f**) spectrum 6.

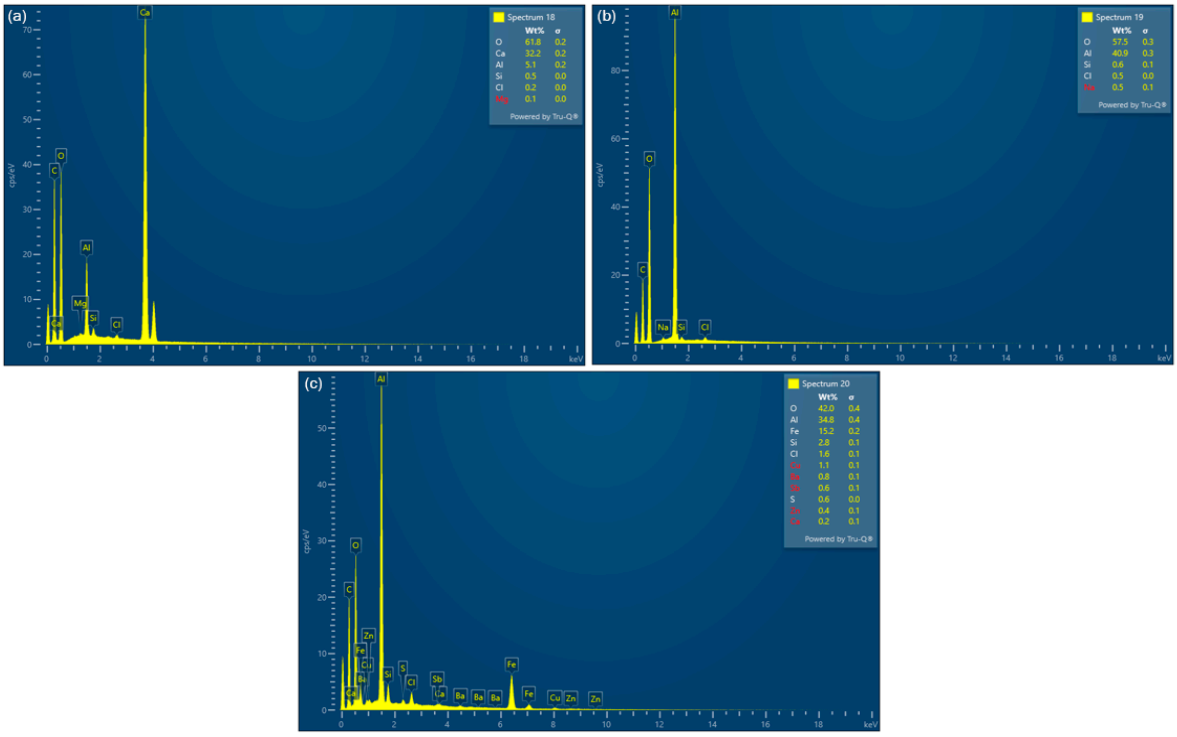

Figure A4. Quantitative EDS of polished samples (30 min; 50 °C, 5 g/L) (**a**) spectrum 18, (**b**) spectrum 19, (**c**) spectrum 20.

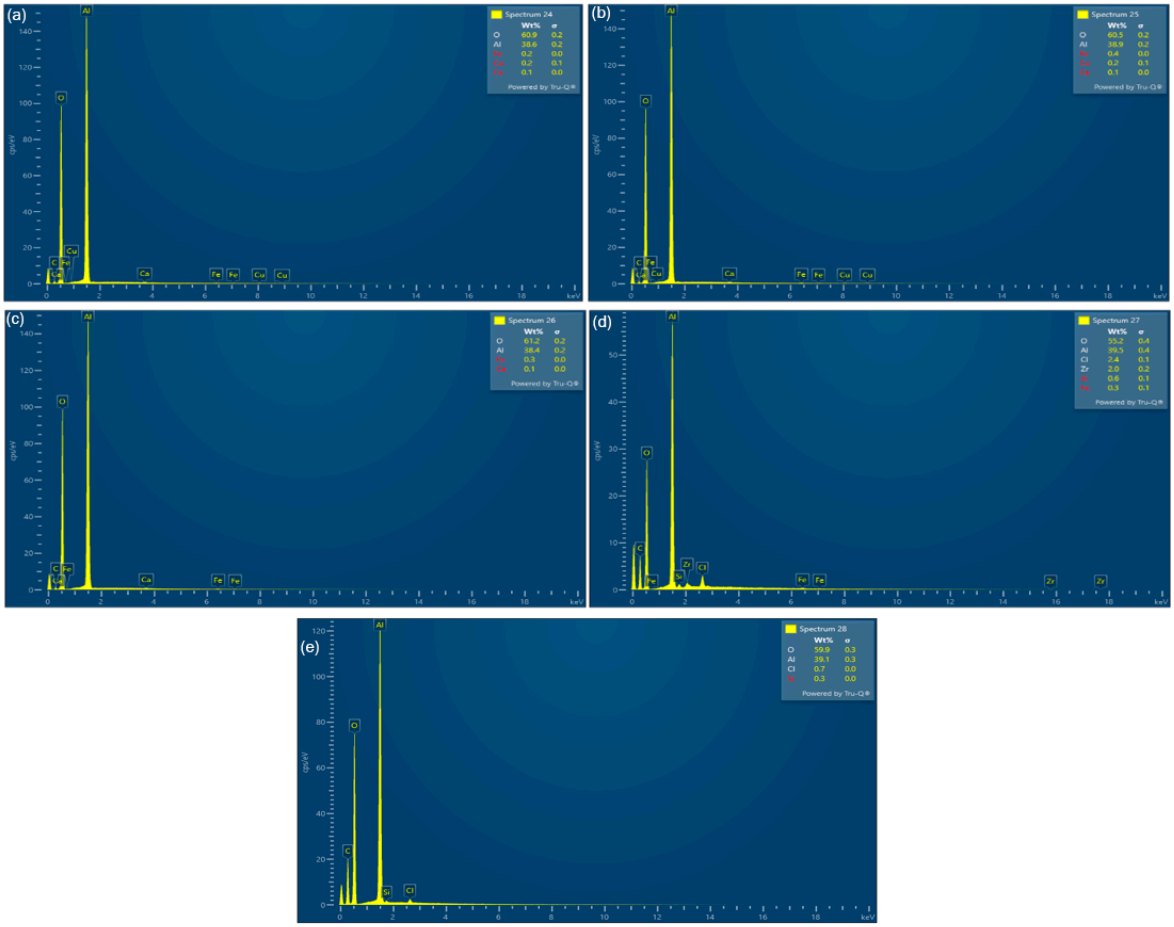

Figure A5. Quantitative EDS of polished samples (30 min, 50 °C, 5 g/L) (**a**) spectrum 24, (**b**) spectrum 25, (**c**) spectrum 26, (**d**) spectrum 27, (**e**) spectrum 28.

References

1. Kvande, H.; Drabløs, P.A. The Aluminum Smelting Process and Innovative Alternative Technologies. *J. Occup. Environ. Med.* **2014**, *56*, S23–S32. [CrossRef] [PubMed]
2. Kloprogge, J.T.; Duong, L.V.; Wood, B.J.; Frost, R.L. XPS Study of the Major Minerals in Bauxite: Gibbsite, Bayerite and (Pseudo-)Boehmite. *J. Colloid Interface Sci.* **2006**, *296*, 572–576. [CrossRef] [PubMed]
3. Donoghue, A.M.; Frisch, N.; Olney, D. Bauxite Mining and Alumina Refining: Process Description and Occupational Health Risks. *J. Occup. Environ. Med.* **2014**, *56*, S12–S17. [CrossRef] [PubMed]
4. Gupta, C.K.; Mukherjee, T.K. *Hydrometallurgy in Extraction Processes, Volume I*; Routledge: London, UK, 2019. [CrossRef]
5. Brough, D.; Jouhara, H. The Aluminium Industry: A Review on State-of-the-Art Technologies, Environmental Impacts and Possibilities for Waste Heat Recovery. *Int. J. Thermofluids* **2020**, *1–2*, 100007. [CrossRef]
6. Habashi, F. A Hundred Years of the Bayer Process for Alumina Production. In *Essential Readings in Light Metals*; Springer: Cham, Switzerland, 2016; Volume 81, pp. 85–93. [CrossRef]
7. Zhang, Y.; Qi, Y.; Li, J.; Zhang, Y.; Qi, Y.; Li, J. Aluminum Mineral Processing and Metallurgy: Iron-Rich Bauxite and Bayer Red Muds. In *Aluminium Alloys and Composites*; Intechopen: London, UK, 2018. [CrossRef]
8. Medvedev, V.V.; Akhmedov, S.N. Evolution of the Technology for the Production of Alumina from Bauxites. In *TMS Light Metal*; Springer: Cham, Switzerland, 2014; pp. 5–9. [CrossRef]
9. Rosenberg, S. Impurity Removal in the Bayer Process. In Proceedings of the 35th International ICSOBA Conference, Hamburg, Germany, 2–5 October 2017.
10. Park, N.K.; Choi, H.Y.; Kim, D.H.; Lee, T.J.; Kang, M.; Lee, W.G.; Kim, H.D.; Park, J.W. Purification of $Al(OH)_3$ Synthesized by Bayer Process for Preparation of High Purity Alumina as Sapphire Raw Material. *J. Cryst. Growth* **2013**, *373*, 88–91. [CrossRef]
11. Li, X.B.; Yan, L.; Zhao, D.F.; Zhou, Q.S.; Liu, G.H.; Peng, Z.H.; Yang, S.S.; Qi, T.G. Relationship between $Al(OH)_3$ Solubility and Particle Size in Synthetic Bayer Liquors. *Trans. Nonferrous Met. Soc. China* **2013**, *23*, 1472–1479. [CrossRef]
12. Noworyta, A. On the Removal of Silica from Aluminate Solutions: Mechanism and Kinetics of the Process. *Hydrometallurgy* **1981**, *7*, 99–106. [CrossRef]

13. Liu, R.; Hou, H.; Lin, Y.; Yan, W.; Hu, X.; Zi, F. Study on the Efficient Removal of Trace Iron from Sodium Aluminate Solution by the Heterogeneous Nucleation Method. *Chem. Eng. Sci.* **2024**, *316*, 121993. [CrossRef]
14. Xu, L.; Chen, W.M.; Zhang, Y.J.; Fan, S.; Pi, J.Q.; Wang, M. li Effect of Zinc(II) and Caustic Content on the Decomposition of Sodium Aluminate Solutions and Relevance to the Bayer Process. *Hydrometallurgy* **2024**, *225*, 106287. [CrossRef]
15. Han, D.Z.; Song, E.W.; Qi, L.J.; Guan, X.G. Optimization of Zinc Removal Process in Sodium Aluminate Solution Based on Orthogonal Experiment. In *Light Metals 2021*; The Minerals, Metals & Materials Series; Springer: Cham, Switzerland, 2021; Volume 6, pp. 31–35. [CrossRef]
16. Vaughan, J.; Peng, H.; Seneviratne, D.; Hodge, H.; Hawker, W.; Hayes, P.; Staker, W. The Sandy Desilication Product Process Concept. *JOM* **2019**, *71*, 2928–2935. [CrossRef]
17. Vind, J.; Vassiliadou, V.; Panias, D. Distribution of Trace Elements Through the Bayer Process and Its By-Products. In Proceedings of the 35th International ICSOBA Conference, Hamburg, Germany, 2–5 October 2017.
18. Ran, J.; Duan, H.; Srinivasakannan, C.; Yao, J.; Yin, S.; Zhang, L. Effective Removal of Organics from Bayer Liquor through Combined Sonolysis and Ozonation: Kinetics and Mechanism. *Ultrason. Sonochem.* **2022**, *88*, 106106. [CrossRef] [PubMed]
19. Lamerant, J.-M.; Air, B. Process for Removing Iron in Sodium Aluminate Liquors Obtained from Alkaline Attack of Bauxite Containing Alumina Monohydrate. U.S. Patent 5,628,972, 13 May 1997.
20. Siziakova, E.; Ivanov, P.; Maximova, R. Feasibility of Applying Alkaline-Earth Metal Carboaluminates for Bayer Process Aluminate Solution Purification from Organic Impurities. *Mater. Sci. Forum* **2021**, *1031*, 109–116. [CrossRef]
21. Liu, J.; Pan, X.; Chen, M.; Yu, H. A Single-Step Crystallization Process to Remove Potassium from Sodium Aluminate Solution. *J. Environ. Chem. Eng.* **2024**, *12*, 113330. [CrossRef]
22. Damjanović, V.; Kostić, D.; Ostojić, Ž.; Perušić, M.; Filipović, R.; Oljača, D.; Obrenović, Z.; Mićić, V. AA21-The Influence of Process Parameters on Removing Iron, Zinc and Copper Impurities from Synthetic Bayer Liquor. In Proceedings of the 38th International ICSOBA Conference, Virtual Conference, 16–18 November 2020; pp. 16–18.
23. The, P. Removal of Copper and Zinc Species from Bayer Process Liquor by Filtration. U.S. Patent 4,414,115, 8 November 1983.
24. Milovanović, B.; Oljača, Đ.; Pavlović, S.; Ostojić, G.; Obrenović, Z. Alumina Production from Purified Bayer Liquor. In Proceedings of the 26th Croatian Meeting of Chemists and Chemical Engineers, Šibenik, Croatia, 9–12 April 2019.
25. Damjanovic, V.; Filipovic, R.; Obrenovic, Z.; Perusic, M.; Kostic, D.; Smiljanic, S.; Stopic, S. Influence of Process Parameters in Three-Stage Purification of Aluminate Solution and Aluminum Hydroxide. *Metals* **2023**, *13*, 1816. [CrossRef]